Supplement of Biogeosciences, 19, 5199–5219, 2022
https://doi.org/10.5194/bg-19-5199-2022-supplement

Biogeosciences Open Access EGU

Supplement of

Eddy-enhanced primary production sustains heterotrophic microbial activities in the Eastern Tropical North Atlantic

Quentin Devresse et al.

Correspondence to: Quentin Devresse (qdevresse@geomar.de)

Supplementary information

Stations localization

Eddies are commonly located and constrained using satellite altimetry data (e.g. CMEMS, https://marine.copernicus.eu). Yet, satellite data are an orientation but often not satisfying to locate eddies for dedicated biogeochemical sampling (Fischer et al. 2021; Fischer et al. in preparation). To estimate the physical properties of the cyclonic eddy in our study, we used multi-section velocity data from a vessel-mounted Acoustic Doppler Current Profiler (vmADCP) data. Following previous studies (Castelão and Johns, 2011; Castelao and He, 2013; Bendinger et al. in preparation), we apply a nonlinear least-squares optimization to reconstruct the eddy within a cylindrical coordinate framework (Fig. **S1**). Briefly, assuming a radially axisymmetric, non-translating vortex the methodology optimizes the azimuthal velocity while coming up with an eddy center estimate. The estimated eddy center is then used to derive the radial azimuthal velocity structure before determining its radius and maximum azimuthal velocity. This characterization is based on the assumption of solid-body rotation, meaning that the azimuthal velocity linearly increases from the center toward the core-periphery (maximum swirl velocity, R1). Outside, toward the eddy periphery (R0), the velocity structure may be defined by a hyperbolic or exponential decay.

The radial structure of azimuthal velocity v_θ is given by

$$v_\theta = -u\sin(\theta) + v\cos(\theta),$$

where u and and v are the zonal and meridional velocities as measured by the vmADCP, and $\theta = \arctan((y - y_c)/(x - x_c))$ with (x, y) the position vectors of the velocity samples and (x_c, y_c) the eddy center coordinates. In the framework of solid-body rotation, the relative vorticity ζ_z is given by

$$\zeta_z = \frac{1}{r}\frac{\partial(r v_\theta)}{\partial r}$$

where r is the radius. The eddy periphery R0 is defined where $\zeta_z = 0$, i.e $\frac{\partial v_\theta}{\partial r} = -\frac{v_\theta}{r}$.

We determined the eddy center at [18.69 °N, 18.05 °W] with a core radius of 40.5 ± 5.7 km (Fig. S1) on the 22/07/19. However, the estimations of the eddy periphery from the three vmADCP sections showed high variability with a radius of the eddy periphery (R0) ranging

between 70 and 90km. Therefore we decided to define the stations inside the periphery of the eddy from the eddy-induced variability on surface temperature, salinity and chlorophyll a (Fig. **1b**,**c**,**d**).

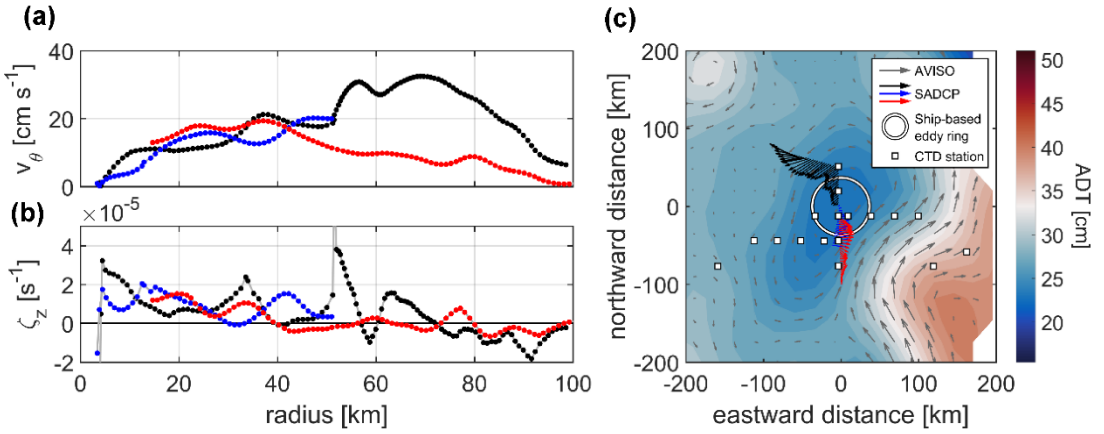

Figure S1: Mean 17.5-49.5 m radial profiles of (a) azimuthal velocity and (b) relative vorticity as a function of radius from the eddy centre as measured and derived by the 75 kHz vmADCP, (c) Background geostrophic velocity field (gray vectors) including absolute dynamics topography (ADT, shading) from 23 July 2019 downloaded from CMEMS. The eddy boundary (defined as the maximum azimuthal velocity) is given by the white circle where the coordinate origin represents the eddy center. Mean 17.5-49.5 velocity vectors for three ship transects across the eddy taking place from 21 July 2019 15:46:00 to 22 July 14:16:00 (black, blue) and from 25 July 2019 15:25 to 25 July 2019 19:47 (red), respectively. Undertaken CTD stations are marked by the white squares.

Taking into account the movement of the CE with an average speed of 3 km d^{-1} (Schütte et al. 2016), and the sampling date, the stations within the core-periphery were characterized as "core" and those outside the core and within the eddy-influenced area as "periphery" (Table **S1**). An anticyclonic eddy was forming along the Mauritanian Coast (core, 17.7°N, 17°W) and was interfering with the velocity field of the CE (Fischer et al. 2021; Fischer et al. in preparation). As the anticyclonic eddy was not fully detached from the coast we considered the stations within it to be still representative of the coast and we characterize them as "coastal" (Table **S1**). Although not reliable for the exact localization of the cores and diameter of eddies, surface height anomaly showed that St. E3 was in the middle of two cyclonic eddies. Therefore St. E3 was likely to be influenced by the phenomenon of frontogenesis and was characterized as a "Frontal Zone". Stations located offshore not likely to be influenced by eddies were defined as "open ocean".

Table S1: Characteristic of M156 sampling stations PP_{DOC} and PP_{TOT} rates in St EDM-4E and CR and BR rates in St. E5 were measured in different cast.

Station	Date	Time (UTC)	Longitude (°W)	Latitude (°N)	Position	Depth all parameters except CR and PP (m)	PP depth sampled (m)	CR depth sampled (m)	Mixed layer depth (m)	Distance from the eddy center (km)
E1	07/04/2019	07:58	-24,33	18,00	Open ocean	5;25;75;125;200	5;25;75	5;25;75;125	38	>200
S1	07/05/2019	05:00	-23,61	18,00	Open ocean	5;25;75;125;200			42	>200
S2	07/08/2019	04:58	-22,78	18,00	Open ocean	5;25;45;100;200			29	>200
E2	07/07/2019	03:48	-22,00	18,00	Open ocean	5;25;50;100;200	5;25;50	5;25;50;100	40	>200
S3	07/09/2019	05:51	-21,13	18,00	Open ocean	5;25;50;100;200	5;25;50	5;25;50;100	35	>200
S4	15/07/2019	04:00	-20,30	18,00	Open ocean	5;25;35;100;200			25	>200
E3	14/07/2019	04:00	-19,55	18,00	Frontal Zone	5;25;45;90;200	5;25;45	5;25;45;90	24	176
EDZ-1	17/07/2019	20:50	-19,11	18,29	Periphery	5;27;50;100;200			7	118
EDZ-2	17/07/2019	23:55	-18,83	18,29	Periphery	5;15;50;100;200	5;15;50	5;15;50;100	11	92
EDZ-3	19/07/2019	02:10	-18,54	18,29	Periphery	5;25;33;60;150			20	67
EDM-4	19/07/2019	07:30	-18,37	18,58	Core	5;23;40;100;200	5;23;40	5;23;40;100	23	34
EDZ-4	18/07/2019	19:50	-18,26	18,29	Periphery	5;26;35;100;175			21	50
EDM-2E	21/07/2019	19:00	-18,08	19,15	Periphery	5;30;45;100;200			23	48
EDM-5E	24/07/2019	06:35	-18,08	18,29	Periphery	5;20;32;40;100			22	47
EDM 3E	22/07/2019	00:42	-18,08	18,87	Core	5;20;38;50;150			26	16
EDM-6E	23/07/2019	22:18	-18,08	18,00	Periphery	5;25;32;50;200	5;25;32		12	79
EDM 4E	22/07/2019	09:15	-18,08	18,58	Core	5;15;35;60;200		5;15;35;60	19	15
EDM 4E	22/07/2019	08:31	-18,08	18,58	Core		5;33;50		22	15
EDZ-5N	26/07/2019	02:15	-17,97	18,58	Core	5;20;30;100;200	5;20;30	5;20;30;100	19	19
EDZ-6N	26/07/2019	08:55	-17,68	18,58	Periphery	5;14;44;100;200			15	44

Table S1 continued:

Station	Date	Time (UTC)	Longitude (°W)	Latitude (°N)	Position	Depth all parameters except CR and PP (m)	PP depth sampled (m)	CR depth sampled (m)	Mixed layer depth (m)	Distance from the eddy center (km)
EDZ-7N	26/07/2019	22:00	-17,39	18,58	Periphery	5;20;40;75;170		5;20	6	73
EDZ-8N	28/07/2019	06:26	-17,11	18,58	Periphery	5;17;40;125			14	103
S6	29/07/2019	01:17	-16,92	18,00	Coastal	5;28;50;130			20	145
EDZ-10N	27/07/2019	18:07	-16,53	18,58	Coastal	5;20;44;75;119			12	162
E5	27/07/2019	06:00	-16,52	18,17	Coastal	5;20;35;111;150	5;20;35		33	175
E5	29/07/2019	05:42	-16,52	18,17	Coastal			5;35;50	29	175

Table S2: Abundance of eukaryotic picoplankton (Euk Pico G1), eukaryotic nanoplankton (Euk nano G2, Euk nano G3 and chrytophyta G5) and cyanobacteria *Prochlorococcus* (*prochlo*) and *Synechococcus* (*Synecho* G4) during M156. All abundances unit are 10^6 cell L^{-1}.

Station	Depth (m)	Lon (°W)	Lat (°N)	*Prochlo*	Euk pico G1	Euk nano G2	Euk nano G3	*Synecho* G4	Chrypto G5
E1	5	-24,33	18,00	0,27	0,80	1,09	0,02	3,87	0,04
E1	25	-24,33	18,00	2,07	2,72	1,17	0,01	3,92	0,05
E1	75	-24,33	18,00	65,93	73,96	4,58	0,08	0,15	0,03
E1	125	-24,33	18,00		0,93	0,08	0,01	0,04	0,03
E1	200	-24,33	18,00		0,07	0,01	0,00	0,01	0,02
S1	5	-23,61	18,00		1,24	1,05	0,03	4,97	0,06
S1	25	-23,61	18,00		3,77	1,10	0,03	4,98	0,06
S1	75	-23,61	18,00		49,01	3,16	0,05	0,05	0,05
S1	125	-23,61	18,00		1,96	0,18	0,01	0,01	0,01
S1	200	-23,61	18,00		0,06	0,00	0,00	0,01	0,01
S2	5	-22,78	18,00		6,64	2,23	0,08	132,75	1,13
S2	25	-22,78	18,00		46,28	3,20	0,10	113,64	0,98
S2	45	-22,78	18,00	220,26	236,32	10,61	0,21	25,26	0,62
S2	100	-22,78	18,00		4,00	0,28	0,01	0,19	0,05
S2	200	-22,78	18,00		0,15	0,01	0,00	0,10	0,01
E2	5	-22,00	18,00	10,30	8,19	4,25	0,10	59,70	0,40
E2	25	-22,00	18,00	7,40	8,13	4,21	0,07	59,24	0,36
E2	50	-22,00	18,00	64,61	94,52	10,44	0,13	44,20	0,40
E2	100	-22,00	18,00		0,89	0,21	0,00	0,57	0,04
E2	200	-22,00	18,00		0,12	0,05	0,00	0,15	0,07
S3	5	-21,13	18,00	7,87	13,91	7,62	0,10	121,85	0,37
S3	25	-21,13	18,00		44,97	9,19	0,12	93,14	0,30
S3	50	-21,13	18,00		44,48	7,53	0,31	3,03	0,20
S3	100	-21,13	18,00		2,22	0,28	0,00	0,75	0,04
S3	200	-21,13	18,00		0,16	0,05	0,00	0,34	0,05
S4	5	-20,30	18,00		14,70	7,14	0,09	314,54	1,11

Table S2 continued:

Station	Depth (m)	Lon (°W)	Lat (°N)	*Prochlo*	Euk pico G1	Euk nano G2	Euk nano G3	*Synecho* G4	Chrypto G5
S4	25	-20,30	18,00		17,08	6,33	0,10	270,50	0,97
S4	35	-20,30	18,00		51,99	7,51	0,33	99,73	0,73
S4	100	-20,30	18,00		1,21	0,18	0,01	0,34	0,05
S4	200	-20,30	18,00		0,17	0,04	0,00	0,51	0,03
E3	5	-19,55	18,00	0,32	5,69	9,92	0,42	14,47	1,44
E3	25	-19,55	18,00	3,07	7,56	6,87	0,51	10,68	0,95
E3	45	-19,55	18,00	13,62	18,08	6,47	0,24	16,70	0,66
E3	90	-19,55	18,00		0,51	0,45	0,03	0,69	0,08
E3	200	-19,55	18,00		0,17	0,04	0,00	0,36	0,03
EDZ-1	5	-19,11	18,29	0,32	0,69	1,27	0,16	19,93	1,02
EDZ-1	27	-19,11	18,29	0,90	2,87	1,42	0,27	12,39	1,71
EDZ-1	50	-19,11	18,29	0,33	2,23	0,43	0,01	1,08	0,21
EDZ-1	100	-19,11	18,29		0,37	0,13	0,01	0,49	0,15
EDZ-1	200	-19,11	18,29		0,27	0,03	0,01	0,40	0,10
EDZ-2	5	-18,83	18,29		1,00	1,75	0,15	37,43	0,76
EDZ-2	15	-18,83	18,29		1,32	2,42	0,23	62,77	1,32
EDZ-2	50	-18,83	18,29		1,31	0,33	0,01	1,48	0,15
EDZ-2	100	-18,83	18,29		0,29	0,09	0,01	0,88	0,12
EDZ-2	200	-18,83	18,29		0,21	0,05	0,00	0,54	0,04
EDZ-3	5	-18,54	18,29		0,99	1,46	0,14	21,84	0,73
EDZ-3	25	-18,54	18,29		1,83	0,56	0,04	4,75	0,50
EDZ-3	33	-18,54	18,29		1,28	0,37	0,01	3,05	0,23
EDZ-3	60	-18,54	18,29		0,55	0,12	0,00	1,27	0,12
EDZ-3	150	-18,54	18,29		0,21	0,03	0,00	0,21	0,05
EDM-4	5	-18,37	18,58		19,60	6,08	0,75	360,78	5,88
EDM-4	23	-18,37	18,58		20,27	5,83	0,68	349,98	5,92
EDM-4	40	-18,37	18,58		3,38	1,59	0,05	11,19	0,50
EDM-4	100	-18,37	18,58		0,20	0,05	0,00	0,62	0,04

Table S2 continued:

Station	Depth (m)	Lon (°W)	Lat (°N)	*Prochlo*	Euk pico G1	Euk nano G2	Euk nano G3	*Synecho* G4	Chrypto G5
EDM-4	200	-18,37	18,58		0,15	0,03	0,00	0,38	0,04
EDZ-4	5	-18,26	18,29		14,11	1,05	0,25	78,46	1,30
EDZ-4	26	-18,26	18,29		17,12	1,78	0,21	81,37	3,39
EDZ-4	35	-18,26	18,29		1,52	0,48	0,03	1,73	0,22
EDZ-4	100	-18,26	18,29		0,28	0,07	0,01	0,68	0,09
EDZ-4	175	-18,26	18,29		0,21	0,03	0,00	0,31	0,04
EDM-2E	5	-18,08	19,15		9,25	4,00	0,68	161,39	1,42
EDM-2E	30	-18,08	19,15		6,44	2,85	0,67	59,56	1,76
EDM-2E	45	-18,08	19,15		12,59	1,62	0,03	2,01	0,16
EDM-2E	100	-18,08	19,15		0,30	0,05	0,01	0,16	0,10
EDM-2E	200	-18,08	19,15		0,34	0,10	0,01	0,23	0,09
EDM-5E	5	-18,08	18,29		9,74	6,19	0,55	223,60	8,16
EDM-5E	20	-18,08	18,29		19,21	2,81	0,17	79,31	2,75
EDM-5E	32	-18,08	18,29		0,99	0,61	0,03	2,99	0,29
EDM-5E	40	-18,08	18,29		1,20	0,41	0,01	1,41	0,16
EDM-5E	100	-18,08	18,29		0,24	0,04	0,00	0,45	0,07
EDM-3E	5	-18,08	18,87		20,93	7,64	1,11	387,07	4,41
EDM-3E	20	-18,08	18,87		20,62	7,48	1,04	327,21	4,51
EDM-3E	38	-18,08	18,87		3,08	5,87	0,09	11,54	0,68
EDM-3E	50	-18,08	18,87		0,35	0,42	0,02	0,94	0,10
EDM-3E	150	-18,08	18,87		0,22	0,07	0,00	0,42	0,06
EDM-6E	5	-18,08	18,00		6,91	6,57	0,11	123,33	0,61
EDM-6E	25	-18,08	18,00		17,98	11,16	0,27	363,00	4,56
EDM-6E	32	-18,08	18,00		19,37	11,75	0,32	377,85	5,18
EDM-6E	50	-18,08	18,00		1,47	0,79	0,05	2,31	0,27
EDM-6E	200	-18,08	18,00		0,18	0,05	0,00	0,51	0,08
EDM-4E	5	-18,08	18,58		33,52	8,91	0,34	621,81	8,25
EDM-4E	15	-18,08	18,58		29,42	7,47	0,29	415,08	5,79

Table S2 continued:

Station	Depth (m)	Lon (°W)	Lat (°N)	*Prochlo*	Euk pico G1	Euk nano G2	Euk nano G3	*Synecho* G4	Chrypto G5
EDM-4E	35	-18,08	18,58		2,43	2,35	0,03	4,49	0,27
EDM-4E	60	-18,08	18,58		0,32	0,19	0,01	0,86	0,08
EDM-4E	200	-18,08	18,58		0,17	0,05	0,00	0,31	0,06
EDZ-5N	5	-17,97	18,58		67,33	8,96	0,39	741,36	10,14
EDZ-5N	20	-17,97	18,58		45,39	5,78	0,40	458,39	8,94
EDZ-5N	30	-17,97	18,58		0,72	1,27	0,07	3,03	0,35
EDZ-5N	100	-17,97	18,58		0,19	0,05	0,01	0,66	0,05
EDZ-5N	200	-17,97	18,58		0,17	0,02	0,00	0,69	0,08
EDZ-6N	5	-17,68	18,58		11,86	4,35	0,35	267,15	4,57
EDZ-6N	14	-17,68	18,58		8,53	1,48	0,16	31,98	1,86
EDZ-6N	44	-17,68	18,58		0,51	0,84	0,01	2,28	0,18
EDZ-6N	100	-17,68	18,58		0,25	0,11	0,00	2,12	0,13
EDZ-6N	200	-17,68	18,58		0,17	0,07	0,00	0,81	0,05
EDZ-7N	5	-17,39	18,58		1,80	2,33	0,59	274,47	1,41
EDZ-7N	20	-17,39	18,58		7,50	1,88	0,45	273,86	1,59
EDZ-7N	40	-17,39	18,58		0,35	0,40	0,03	3,51	0,23
EDZ-7N	75	-17,39	18,58		0,28	0,10	0,00	3,56	0,15
EDZ-7N	170	-17,39	18,58		0,17	0,03	0,01	1,28	0,08
EDZ-8N	5	-17,11	18,58		2,95	6,58	0,39	642,99	2,80
EDZ-8N	17	-17,11	18,58		14,81	10,72	0,54	1079,84	6,01
EDZ-8N	40	-17,11	18,58		0,41	0,30	0,01	1,12	0,17
EDZ-8N	125	-17,11	18,58		0,31	0,12	0,00	1,90	0,12
S6	5	-16,92	18,00		9,32	4,91	0,19	13,11	0,31
S6	28	-16,92	18,00		40,19	17,29	0,20	24,59	0,39
S6	50	-16,92	18,00		17,20	13,21	0,13	72,63	1,06
S6	130	-16,92	18,00		1,95	0,53	0,01	1,60	0,09
EDZ-10N	10	-16,53	18,58		3,16	2,39	0,05	48,53	0,33
EDZ-10N	20	-16,53	18,58		3,63	2,31	0,03	57,46	0,29

Table S2 continued:

Station	Depth (m)	Lon (°W)	Lat (°N)	*Prochlo*	Euk pico G1	Euk nano G2	Euk nano G3	*Synecho* G4	Chrypto G5
EDZ-10N	44	-16,53	18,58		78,20	13,03	0,18	102,19	2,15
EDZ-10N	75	-16,53	18,58		7,10	1,45	0,02	3,16	0,16
EDZ-10N	119	-16,53	18,58		0,59	0,20	0,01	2,24	0,19
E5	5	-16,52	18,17	4,37	5,97	1,56	0,05	63,10	0,46

Community respiration using the optode-based method

The most used technique to determine the trophic state of a system (autotrophy or heterotrophy) is the Winkler method with dark-light bottle incubation from which gross primary production and community respiration rates ratio is obtained (GPP/CR; e.g. Regaudie-de-Gioux et al. 2012). But the Winkler method is time-consuming and to study BR, a filtration step is mandatory which causes two major problems, oxygen contamination of the samples and an overestimation of BR by removing the protistan grazer (Aranguren-Gassis et al. 2012). Shorter incubation with *in-vivo* ETS method (Martínez-García et al. 2009) reducing filtration impacts had shown that Community respiration (CR) and BR are tightly correlated even in the oligotrophic area (Aranguren-Gassis et al. 2012). However, such techniques still distort water oxygen properties and therefore are not suitable when it comes to investigating oxygen minimum zones, which occurred in our case. Optode-method was therefore a suitable option in terms of precision, rapidity of implementation, and ability to maintain water properties.

Optodes were glued to the inside surfaces of Winkler-bottles using silicone cement (Warkentin et al. 2007). We allowed the silicone to cure for 2 days at room temperature. Before the cruise, we performed a two-point calibration of optodes according to the manufacturer's instructions using air-saturated and temperature-equilibrated samples and oxygen-depleted samples obtained by dissolving Na_2SO_3 into Milli-Q water (10g L^{-1}). We measured the photoluminescence lifetime of the luminophores within sensor spots by a fiber-optic oxygen meter (Fibox 3; PreSens GmbH) fixed outside of the bottle opposite to inside sensor spots. We supplied excitation light (505 nm), which also transported the emitted fluorescence signal (600 nm) back to the oxygen meter (Warkentin, 2007). We incubated optodes bottles at 14°C in the dark for at least 24h and with at least four-time point measurements. We followed the temperature inside bottles with a Pt100 Temperature Sensor (Presens) to monitor temperature acclimation. Oxygen concentrations were measured every 2s during an interval of 3 to 5 minutes and data were recorded using OxyView 7.01 (PreSens GmbH). Bottles were rinsed between each set of incubations with 4-5% HCL (manufacturer indication) and five times with 18 MΩ Mili-Q. Incubations were initiated by transferring seawater to the glass bottles using standard gas sampling techniques to avoid oxygen contamination. Site-specific values for salinity compensation of the oxygen readings were obtained from cabled CTD casts. Oxygen measurements were corrected using the Presens oxygen calculator with the mean temperature value measured at each time point (in extra temperature-control bottles) and with the *in-situ* salinity to determine the absolute $[O_2]$ values. $[O_2]$ values precision was validated by

comparison of values measured directly after sampling and CTD oxygen data corrected with Winkler titrations (Fig. S**2**) for the same depth.

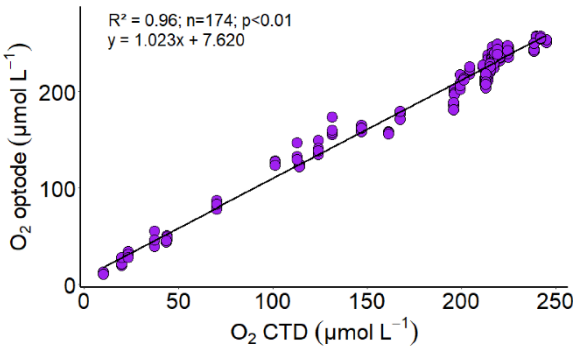

Figure S2: Linear correlation between calibrated oxygen values obtained from the CTD and oxygen concentration measured with optode directly after sampling during the community respiration experiments.

We determined the drift commonly occurring with optode-based methods (Wikner et al. 2013; Vikström et al. 2019) by collecting and filtering seawater through 0.2µm nucleopore filters which were incubated in the dark like the samples. Non-linear oxygen dynamics are frequent in oxygen measurement, (Briand et al. 2004, Vikström et al. 2019) in both natural and manipulated samples. Therefore, Akaike information criteria (AIC; Snipes and Taylor 2014) was used to determine when nonlinear oxygen dynamics occurred. Then a quadratic polynomial (Eq. 1) was fitted to the data:

$$[O_2] = C + at + bt^2 \text{ (Eq. 1)}$$

Here, $[O_2]$ is the absolute oxygen concentration at time t, C the y-axis intercept, and *a* and *b* are coefficients. As oxygen respiration is assumed to be linear, daily CR was calculated using the difference of the linear (or quadratic polynomial) regression between t0 (after temperature acclimation) and 24 h. We obtained a detection limit of CR of 0.62 µmol O_2 L^{-1} d^{-1} by taking the standard error of the oxygen decline (SE_{sample}) and residual standard error in 0.2 µm filtered seawater ($SE_{background}$) into account and using SE_{Total} as a detection limit according to Eq.2:

$$SE_{Total} = \sqrt{SE_{samples}^2 + SE_{background}^2} \text{ (Eq.2)}$$

Extrapolation of ex-situ BP and CR rates at 22°C

As we measured the microbial activities at different incubation temperatures for technical concern, we decided to convert the values of BP and CR at 22°C because we could not successfully extrapolate the PP_{TOT} rates to in-situ temperature. For that we used equations from López-Urrutia and Morán for BP (BP_U; 2007; Eq.5) and from Regaudie de Gioux and Duarte for CR (CR_{RG}; 2012; Eq.7).

$$BP_U = \left[e^{-0.589/(kT)} \times \left[\frac{2.33 \times 10^{11} chl\ a}{chl\ a + 4.08} + 6.77 \times 10^9\right]\right] \times Bacterial\ abundance \quad \text{(Eq. 5)}$$

Temperature and resource availability effects on cell-specific bacterial metabolism, with k, the Boltzmann's constant (8.617734 10^{-5} eV K^{-1}), T the water temperature (°K), chl *a*, the *in-situ* chlorophyll *a* concentration in µg L^{-1} and *in-situ* bacterial abundance in cell L^{-1}.

$$Ln^{(\frac{CR_{RG}}{chl\ a})} = -0{,}66 \times \left(\frac{1}{kT}\right) + 27{,}72 \quad \text{(Eq.6)}$$

$$CR_{RG} = e^{Ln^{(\frac{CR}{chl\ a})}} \times chl\ a \quad \text{(Eq.7)}$$

The linear relationship between the natural logarithm of the volumetric specific chlorophyll a-CR rates ($\frac{CR}{chla}$ in mmol O_2 mg Chl a^{-1} d^{-1}) within 1°C bin and the inverted water temperature (1/kT with k, the Boltzmann's constant (8.617734 10^{-5} eV K^{-1}) and with T, the water temperature (°K)). CR_{RG} (µmol O_2 L^{-1} d^{-1}) was then obtained from the exponential of the natural logarithm of the volumetric specific chlorophyll a-CR rates multiplied by the *in-situ* chlorophyll *a* (Chl *a* in µg L^{-1}).

Then, we compared the rates of BP and CR measured *ex-situ* ($BP_{ex-situ}$ and $CR_{ex-situ}$) with the rates obtained from BP_U and CR_{RG} calculated at the temperature set during the incubations (Fig. **S3**). It was 14°C for BP and for CR (~14°C) they are listed in table **S3**. The rates obtained from the equations (BP_U and CR_{RG}) were significantly correlated (Fig. **S3**) and within the ranges of the rates measured with *ex-situ* incubations ($BP_{ex\text{-}situ}$ and $CR_{ex\text{-}situ}$). Therefore, we used the correlation between BP_U and CR_{RG} rates (Fig. **S3**) calculated at the incubation temperature and at 22°C to extrapolate BP and CR at 22°C:

$$BP_{22°C} = BP_{14°C} \times 0{,}996$$

$$CR_{22°C} = CR_{14°C} \times 2.011 - 0.013$$

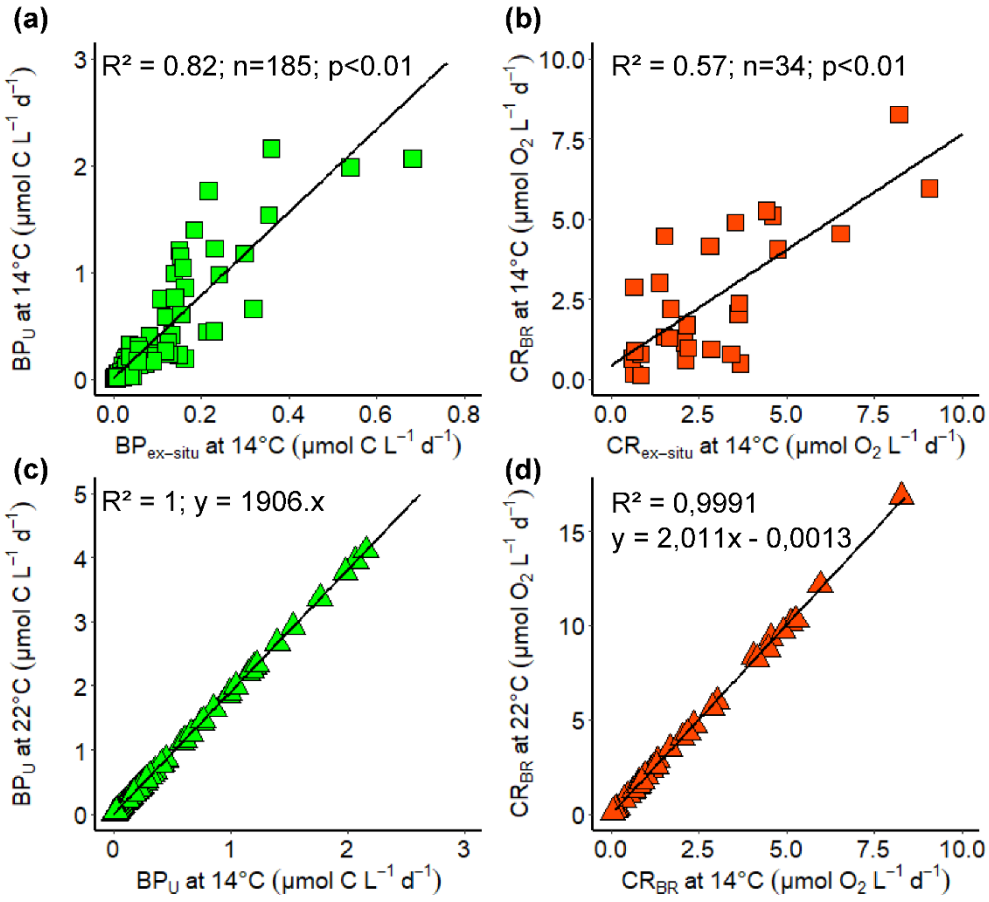

160

161 Figure S3: Linear relationship between BP_U and CR_{RG} rates calculated at the temperature measured
162 during *ex-situ* incubation (14°C for BP, see table **S2** for CR) and the ex-situ BP (**a**) and CR rates (**b**) and
163 linear relationship between BP_U and CR_{RG} rates calculated at the temperature measured during *ex-situ*
164 incubation (14°C for BP, see table **S2** for CR) and 22°C, (**c**) and (**d**).

165

Table S3: Average and standard deviation (SD) of temperature measured during community respiration experiments.

Station	Depth (m)	Incubation temperature		Station	Depth (m)	Incubation temperature	
		Average	SD			Average	SD
E1	5	13,91	0,12	EDM-4	5	14,43	0,01
	25	13,86	0,14		23	14,43	0,03
	75	13,90	0,13		40	14,40	0,03
	125	13,86	0,17		100	14,42	0,04
E2	5	14,13	0,10	EDM-4E	5	14,55	0,02
	25	14,15	0,09		15	14,56	0,02
	50	14,17	0,12		35	14,56	0,02
	100	14,15	0,12		60	14,55	0,01
S3	5	13,55	0,15	EDZ-5N	5	14,43	0,12
	25	13,56	0,16		20	14,41	0,12
	50	13,59	0,19		32	14,42	0,11
	100	13,53	0,15		100	14,39	0,13
E3	5	14,01	0,05	EDZ-7N	5	14,33	0,06
	25	13,96	0,06		25	14,35	0,06
	45	13,98	0,06	E5	5	14,49	0,05
	90	14,02	0,06		15	14,49	0,04
EDZ-2	5	14,10	0,05		35	14,49	0,05
	15	14,10	0,05				
	50	14,09	0,05				
	100	14,10	0,05				

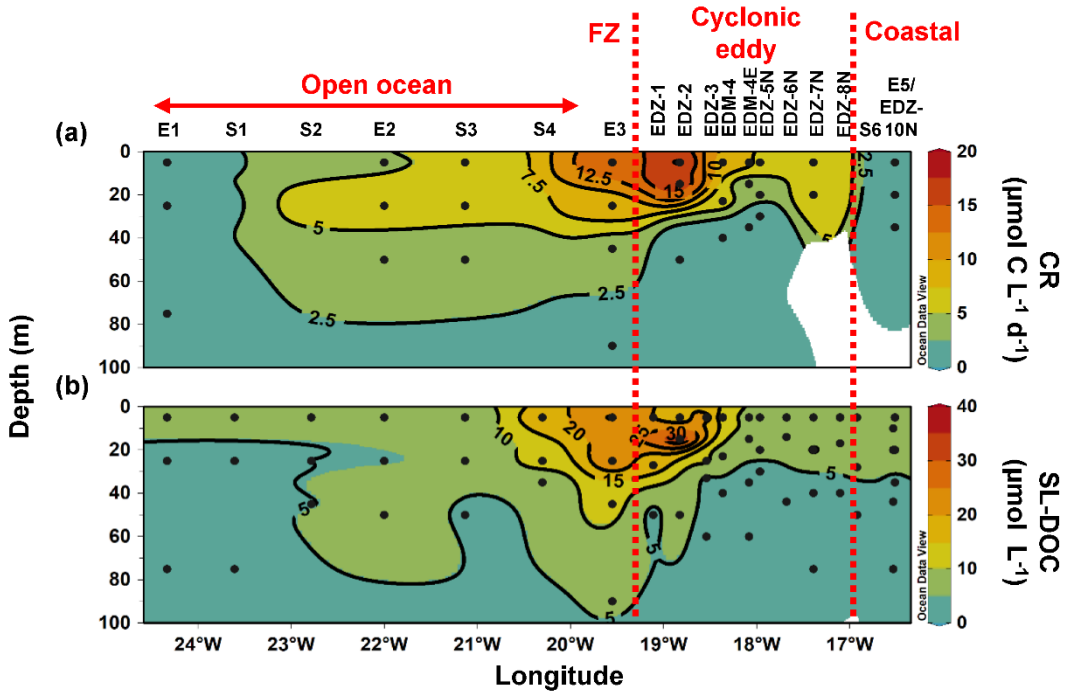

Figure S4: depth distribution of (**a**) community respiration and (**b**) Semi-labile dissolve organic carbon (SLDOC) over 100m depth. Red dashed line show the eddy-influenced area and FZ refer as Frontal Zone.

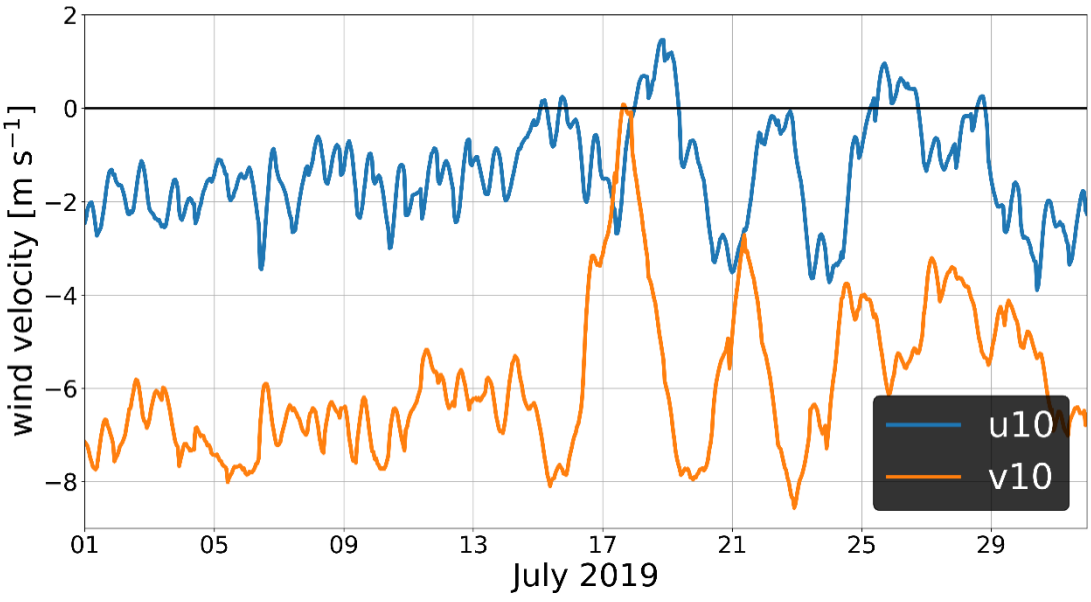

Figure S5: Domain averaged (25W-16W, 16N-22N) eastward (u10) and northward (v10) component of the 10m wind. Data were obtained from ERA5 database (Hersbach et al., 2018)

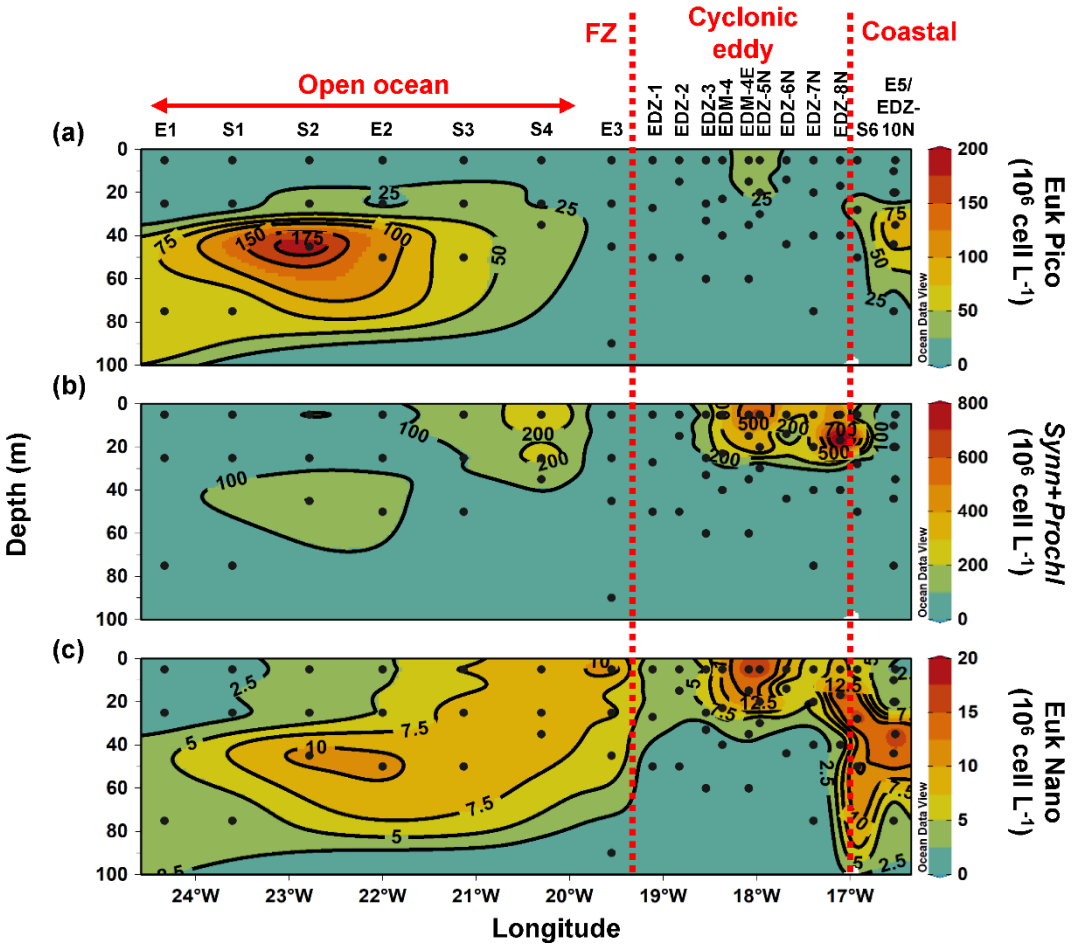

Figure S6: depth distribution of (**a**) eukaryotic picoplankton abundance, (**b**) sum of cyanobacteria *prochlorococcus* and *synechococcus* abundance, (**c**) sum of eukaryotic nanoplankton abundance (G2 and G3 and chryptophyta) over 100m depth. Red dashed line show the eddy-influenced area and FZ refer as Frontal Zone. see SI Table **2** for details.

185 Reference
186

187 Aranguren-Gassis, M., Teira, E., Serret, P., Martínez-García, S., and Fernández, E.: Potential
188 overestimation of bacterial respiration rates in oligotrophic plankton communities, Mar. Ecol.
189 Prog. Ser., 453, 1–10, https://doi.org/10.3354/meps09707, 2012.

190 Briand, E., Pringault, O., Jacquet, S., and Torréton, J. P.: The use of oxygen microprobes to
191 measure bacterial respiration for determining bacterioplankton growth efficiency. Limnol.
192 Oceanogr. Methods, 2(12), 406–416, https://doi.org/10.4319/lom.2004.2.406, 2004.

193 Castelão, G. P., and Johns, W. E.: Sea surface structure of North Brazil Current rings derived
194 from shipboard and moored acoustic Doppler current profiler observations. J. Geophys. Res.
195 Oceans, 116(1), 1–12, https://doi.org/10.1029/2010JC006575, 2011.

196 Castelao, R. M., and He, R.: Mesoscale eddies in the South Atlantic Bight. J. Geophys. Res.
197 Oceans, 118, 5720–5731, https://doi.org/10.1002/jgrc.20415, 2013.

198 Fischer, T., Karstensen, J., Dengler, M., and Bendinger, A.: Multiplatform observation of
199 cyclonic eddies during the REEBUS experiment, EGU General Assembly 2021, online, 19–30
200 Apr 2021, EGU21-6537, https://doi.org/10.5194/egusphere-egu21-6537, 2021.

201 Hersbach, H., Bell, B., Berrisford, P., Biavati, G., Horányi, A., Muñoz Sabater, J., Nicolas, J.,
202 Peubey, C., Radu, R., Rozum, I., Schepers, D., Simmons, A., Soci, C., Dee, D., Thépaut, J-N.:
203 ERA5 hourly data on single levels from 1979 to present. Copernicus Climate Change Service
204 (C3S) Climate Data Store (CDS). (Accessed on 08-Oct-2021), 10.24381/cds.adbb2d47, 2018.

205 López-Urrutia, Á., and Morán, X. A. G.: Resource limitation of bacterial production distorts
206 the temperature dependence of oceanic carbon cycling, Ecology, 88(4), 817–822.
207 https://doi.org/10.1890/06-1641, 2007.

208 Martínez-García, S., Fernández, E., Aranguren-Gassis, M., and Teira, E.: In vivo electron
209 transport system activity: A method to estimate respiration in natural marine microbial
210 planktonic communities, Limnol. Oceanogr. Methods, 7, 459–469,
211 https://doi.org/10.4319/lom.2009.7.459, 2009.

212 Regaudie-De-Gioux, A., and Duarte, C. M.: Temperature dependence of planktonic metabolism
213 in the ocean, Glob. Biogeochem. Cycles., 26(1), 1–10. https://doi.org/10.1029/2010GB003907,
214 2012.

Snipes, M., and Taylor, D. C.: Model selection and Akaike Information Criteria: An example from wine ratings and prices, Wine Econ. Policy, 3(1), 3–9. https://doi.org/10.1016/j.wep.2014.03.001, 2014.

Vikström, K., Tengberg, A., & Wikner, J.: Improved accuracy of optode-based oxygen consumption measurements by removal of system drift and nonlinear derivation, Limnol. Oceanogr. Methods, 17(3), 179–189, https://doi.org/10.1002/lom3.10297, 2019.

Warkentin, M., Freese, H. M., Karsten, U., and Schumann, R.: New and fast method to quantify respiration rates of bacterial and plankton communities in freshwater ecosystems by using optical oxygen sensor spots, Appl. Environ. Microbiol, 73(21), 6722–6729, https://doi.org/10.1128/AEM.00405-07, 2007.

Wikner, J., Panigrahi, S., Nydahl, A., Lundberg, E., Båmstedt, U., and Tengberg, A.: Precise continuous measurements of pelagic respiration in coastal waters with Oxygen Optodes. Limnol. Oceanogr. Methods, 11, 1–15, https://doi.org/10.4319/lom.2013.11.1, 2013.